

# Thermophysical, mechanical and dielectric studies on piperidinium *p*-hydroxybenzoate

## A novel organic NLO single crystal

G. Shanmugam · K. Thirupugalmani ·  
R. Rakhikrishna · J. Philip · S. Brahadeeswaran

Received: 24 January 2013 / Accepted: 22 March 2013 / Published online: 16 April 2013  
© Akadémiai Kiadó, Budapest, Hungary 2013

**Abstract** Single crystals of recently identified nonlinear optical material, piperidinium *p*-hydroxybenzoate (PDPHB), were grown by solution cooling method. It crystallizes in a monoclinic system with a noncentrosymmetric space group Cc. Thermal stability and decomposition behavior of PDPHB are illustrated through thermogravimetric, differential thermal and differential calorimetric analysis. The thermal diffusivity, thermal conductivity, and specific heat capacity of the grown crystals, which are the three most important thermo-physical parameters in heat transfer calculations, are calculated by an improved photopyroelectric technique. The room temperature hardness test has been performed on crystallographic planes (200), (020), and (002) using Vickers microhardness tester and the results are analyzed through the classical Meyer's law. The dielectric constant, dielectric loss, and ac conductivity are studied as a function of frequency (100 Hz to 1 MHz) and temperature (313–363 K). All these studies are performed for the first time and aimed to explore the useful and safe region of thermal, mechanical, and electrical properties to enhance effectiveness of PDPHB crystals for device fabrications.

**Keywords** Optical materials · TG/DTA · DSC · Specific heat · Photopyroelectric

## Introduction

Single crystals with enhanced second harmonic generation (SHG) efficiency have been investigated for the past three decades due to their active contribution in modern fields like non-linear optics (NLO), Terahertz wave technology, and Electro optics, etc. [1–4]. As these applications are based on various physicochemical properties of materials such as transparency, molecular nonlinearity, thermal and dielectric behavior, organic materials are mostly favored to realize them. Moreover, they offer numerous design possibilities, larger optical nonlinearities, and faster responses when compared to their inorganic counterparts [4]. In general, carboxylic acids have been used as primary building blocks in the design of crystal structures by exhibiting characteristic intermolecular interactions and aggregation patterns. Due to its strength and directionality, hydrogen bonding is perhaps the most reliable design element in the directed self-assembly of small organic molecules with hydrogen bond donor and acceptor functionalities. As a good hydrogen bond donor, *p*-hydroxybenzoic acid (phenolic derivative of benzoic acid) has been established as the most effective tool in crystal engineering. In this direction, we have recently identified piperidinium *p*-hydroxybenzoate (PDPHB) as an NLO material, which constitutes hydrogen bonded benzoic acid (as anion) with piperidine (as cation). The growth, quantum chemical, and spectroscopic characterizations were reported elsewhere [5], and it has been shown that large size and optical quality single crystals of PDPHB can be grown from the saturated solution under optimized growth conditions. The UV–visible cutoff wavelength, optical transparency, and band gap were found to be about 300 nm, 91 %, and 4.03 eV, respectively. The experimental second harmonic generation efficiency of PDPHB was nearly 19 and 2.41 times greater than that of standard KH<sub>2</sub>PO<sub>4</sub> and urea,

G. Shanmugam · K. Thirupugalmani · S. Brahadeeswaran (✉)  
Department of Physics, Anna University, BIT Campus,  
Tiruchirappalli 620 024, India  
e-mail: sbrag67@yahoo.com

R. Rakhikrishna · J. Philip  
Department of Instrumentation, Cochin University of Science  
and Technology, Cochin 682 022, India

respectively. Emphatically, the prolificacy of PDPHB such as its non-hygroscopic/-hydrated/-cleavage character, admirable optical transparency, and high second harmonic generation efficiency persuaded us to continue our investigations on some of its thermophysical and physicochemical properties. Herein, we report the studies of thermogravimetric/differential thermal analysis (TG/DTA), differential scanning calorimetric (DSC) analysis, thermophysical properties by photopyroelectric (PPE) technique, dielectric behavior and hardness anisotropy of PDPHB in a detailed manner.

## Experimental

### Material synthesis and crystal growth

PDPHB was synthesized from equimolar quantities of highly pure piperidine ( $C_5H_{11}N$ ) (Merck) and *p*-Hydroxybenzoic acid ( $C_7H_6O_3$ ) (Aldrich), by using ethanol (Hayman) as a solvent. The PDPHB has been reported to crystallize in the noncentrosymmetric monoclinic space group *Cc* with four molecules in asymmetric unit [6]. Nonius CAD-4/MACH 3 Diffractometer, with  $MoK\alpha$  radiation ( $0.71073 \text{ \AA}$ ) was used to obtain the accurate cell parameters of the grown crystals at room temperature. Cell parameters were obtained from the least-squares refinement of the setting angles of 25 reflections. The cell parameters obtained from single crystal X-ray diffraction using Nonius CAD-4 diffractometer were:  $a = 6.075(3) \text{ \AA}$ ,  $b = 18.355(4) \text{ \AA}$ ,  $c = 10.201(6) \text{ \AA}$  &  $\beta = 93.11(6)^\circ$ . These results agreed well with the reported values. The adjacent units are interconnected through inter-molecular hydrogen bonding interactions which play major role in the packing arrangement of these molecules inside the unit cell. Bulk growth of PDPHB was achieved by employing a water bath equipped with a programmable Eurotherm temperature controller (3216) having an accuracy of  $\pm 0.01 \text{ }^\circ\text{C}$ . The spontaneously and seeded grown PDPHB crystals are shown in Fig. 1a, b, respectively.

### Characterization techniques

The simultaneous thermo gravimetric analysis (TG) and differential thermal analysis (DTA) were performed on PDPHB powder, using a simultaneous thermal analyzer NETZSCH STA 409 PC/PG (resolution:  $0.002 \text{ mg}$ , reference/crucible: alumina) with a heating rate of  $10 \text{ K min}^{-1}$  from  $33$  to  $450 \text{ }^\circ\text{C}$ . The differential scanning calorimetric (DSC) curve was obtained in the range between  $25$  and  $210 \text{ }^\circ\text{C}$  using METTLER-TOLEDO DSC1 thermal analyzer. The Vickers microhardness behavior was studied using Shimadzu microhardness tester (model: HMV-2T, range:  $98.07 \text{ mN}$  to  $19.6 \text{ N}$ ). The dielectric studies were

carried out as a function of frequency ( $100 \text{ Hz}$  –  $1 \text{ MHz}$ ) and temperature ( $313$ – $363 \text{ K}$ ) using a HIOKI 3532-50 LCR HITESTER. The crystal plates of (020) orientations were coated with Aluminum paste and they were pressed on either side to establish proper contacts.

## Results and discussions

### TG, DTA and DSC studies

The simultaneous TG and DTA were performed on  $6.536 \text{ mg}$  of PDPHB powder sample which was derived from its single crystals and the resultant curves were shown in Fig. 2. They are recorded to analyze the melting and the decomposition behavior of PDPHB so that their thermal treatment region could be defined. The DTA curve revealed that the material undergoes an irreversible endothermic transition at  $150 \text{ }^\circ\text{C}$ , where the melting begins. The peak of the endothermic, which represents the temperature  $170 \text{ }^\circ\text{C}$  at which melting terminates, corresponds to its melting point. The flat response of TG curve up to  $150 \text{ }^\circ\text{C}$  implies non-existence of crystallization solvent or impurity in the crystal structure and most specifically the thermal stability of PDPHB up to the onset of melting. It is the most beneficial property observed for compounds, where the lattice force is more predominating than the covalent bonding forces in the molecules [7]. The shape of the TG curve after its melting represents the thermal decomposition of PDPHB with the formation of volatile reaction products [8]. The single stage complete mass loss from  $150$  to  $240 \text{ }^\circ\text{C}$  illustrates the simultaneous melting and decomposition of the piperidinium and benzoate moiety and also the removal of almost all fragments as gaseous products. The decomposition temperature  $T_d$  was identified as  $223 \text{ }^\circ\text{C}$ , which was estimated as the temperature at the intercept of the leading edge of the mass loss that can involve sublimation and/or decomposition by the base line of the TG scans [9]. The DSC curve recorded with a heating rate of  $10 \text{ }^\circ\text{C min}^{-1}$  is shown in Fig. 3. From the figure, it could be seen that a sharp endothermic peak with an onset, peak maximum and offset occurred at  $150$ ,  $177$ , and  $163 \text{ }^\circ\text{C}$ , respectively. This endothermic peak is assigned to the sample's melting process since it absorbs energy in order to melt. The melting point of PDPHB was recognized as  $150 \text{ }^\circ\text{C}$  in view of the fact that for crystalline samples, the melting point is reflected by the onset temperature, which is where melting begins, and not the peak maximum value [10]. The peak maximum value and the peak height value will be influenced by sample mass and possibly by encapsulation procedure, since poor thermal contact will result in a broader peak with lower peak height [10, 11]. The purity is determined by analyzing the shape of the

**Fig. 1** Typical photograph of **a** spontaneously grown and **b** seeded grown PDPHB single crystal

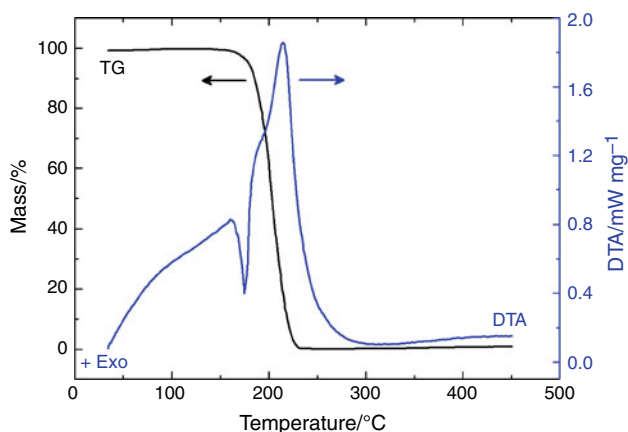
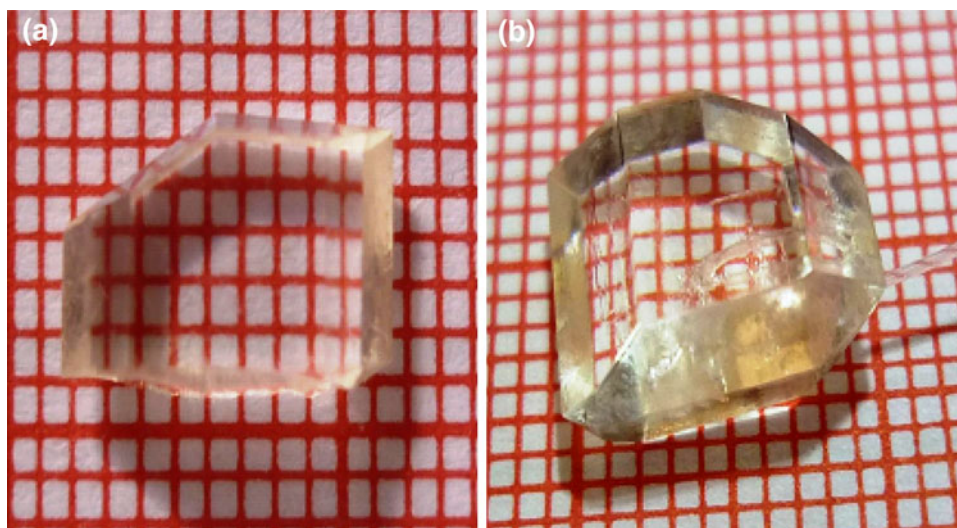


**Fig. 2** TG/DTA curves of PDPHB crystalline powder

melting curve obtained by DSC plot of a given sample. The higher the concentration of an impurity in a given sample, the lower is the melting point and the broader the melting range. Hence, the higher the melting point and the sharpness of DSC melting peak reveal the crystallinity and purity of the sample.

#### Specific heat analysis

For harmonic generation, the conversion efficiency of an NLO crystal is strongly influenced by the intensity of incident laser power. Consequently, its utility for suitable devices depends not only on its linear and nonlinear optical properties but also largely on its ability to withstand high power lasers [12]. Specific heat is one of the important thermophysical parameters that strongly influences the damage threshold and thermal conductivity of a crystal [13]. It is very sensitive to the nature in which the atoms or molecules are dynamically bound in a solid [14]. In general, the specific heat data of solids are described by the Debye

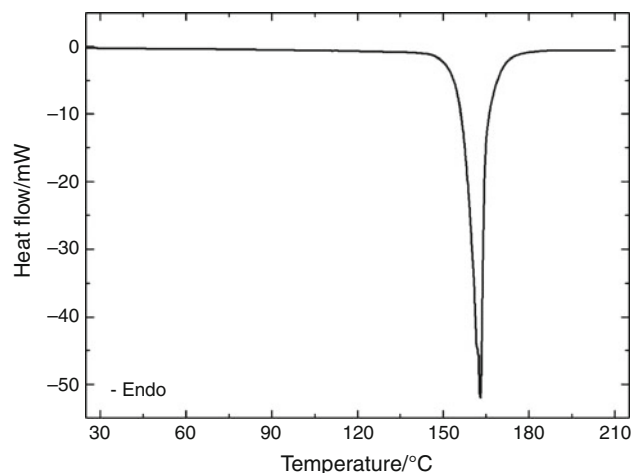


**Fig. 3** Differential scanning calorimetric analysis of PDPHB powder

theory in terms of harmonic frequency spectrum for each crystalline lattice. As PDPHB is an organic crystal, it is very difficult to calculate the specific heat of the bulk material with the prediction of a lattice theory like Debye's due to its complexity [15]. Hence, the specific heat of the powder sample of PDPHB was determined by the modulated differential scanning calorimetric (MDSC) technique with a cooling rate of  $2\text{ }^{\circ}\text{C min}^{-1}$  using METTLER-TOLEDO DSC1 thermal analyzer. The advantages of MDSC over conventional methods have been discussed elsewhere in a detailed manner [16]. In general, when a laser beam passes through the crystal, part of the light will be absorbed by it. This creates a temperature gradient inside the crystal and as a consequence, the thermal expansion could occur [17]. If the crystalline sample exhibits strong anisotropic behavior then the thermal expansion coefficients of the crystal could cause cracks in it. Intuitively, an NLO material with higher specific heat could be expected to be of more resistance to laser damage since a crystal with high specific heat will have

a smaller temperature gradient than a crystal with a low specific heat when absorbing the same quantity of heat [17]. In addition to that, the large temperature gradient disturbs the phase matching properties considerably [18]. Moreover, as for the bulk material, in general, crystal defects may act as the origins for bulk laser damage [19]. The temperature dependency of the specific heat of PDPHB is shown in Fig. 4. From the figure, it can be seen that the specific heat of PDPHB increases linearly (from 4.538 to 6.663 J g<sup>-1</sup> K<sup>-1</sup> in the measured temperature range (300–400 K)) with temperature up to the onset of melting. The specific heat of PDPHB measured by MDSC method at 300 K is about 4.538 J g<sup>-1</sup> K<sup>-1</sup>, which is greater than some of the important NLO crystals (listed in Table 1) such as KDP [20], KTP [20], LN [20], LAP [21], NPNa·2H<sub>2</sub>O [22] and some recently identified NLO crystals like LHPP [1], acetoacetanilide [23], DAPNP [20] at the same temperature. As these NLO materials having high laser damage thresholds (LN, 0.3 GW cm<sup>-2</sup> (10 ns); KDP, 5 GW cm<sup>-2</sup> (1 ns); KTP, 9–20 GW cm<sup>-2</sup> (1 ns); LAP, 13 GW cm<sup>-2</sup> (25 ns); NPNa·2H<sub>2</sub>O, 11.16 GW cm<sup>-2</sup> (8 ns); it could be expected that PDPHB would also possess higher damage threshold [22, 24]. The anomalous variation in specific heat capacity after 425 K may be due to softening of phonon modes and the corresponding enhanced contribution of phonon modes to the specific heat capacity [25]. Moreover, the anhydrous nature of PDPHB is favorably viewed in terms of its thermal stability since prolonged heating of a hydrated crystalline material by laser radiation may promote the liberation of water vapor and hence degrade the structure of the material within.

#### Photopyroelectric studies

The thermo-physical properties of PDPHB single crystals were determined by an improved Photopyroelectric (PPE)

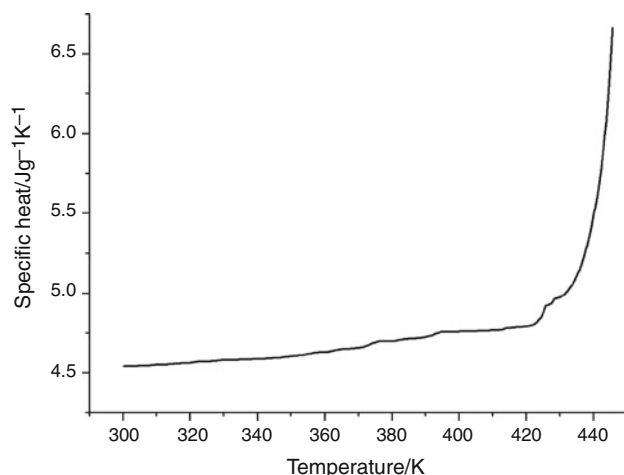


**Fig. 4** Temperature dependence of heat capacity of PDPHB

method [26]. Here, the sample was illuminated by an intensity-modulated beam of light, which gives rise to periodic temperature variation by optical absorption. The thermal waves, thus generated, propagate through the sample and were detected by the pyroelectric detector. For this study, a 28 μm thick Ni–Cr coated polyvinylidene difluoride (PVDF) film, with pyroelectric coefficient  $P = 0.25 \times 10^{-8}$  V cm<sup>-1</sup> K<sup>-1</sup> at room temperature, was used as the pyroelectric detector. The room temperature values of pyroelectric detector resistance and capacitance were 50 GΩ and 750 pF, respectively. A 120 mW He–Cd laser ( $\lambda = 442$  nm) was used as the optical heating source and a mechanical chopper (Model No. SR 540) was used as the intensity modulator of laser beam. As the PDPHB has no phase transition before its melting, which is also substantiated by TG/DTA/DSC analysis, the PPE measurements were limited to room temperature only. A PDPHB crystal was carefully polished using a polishing mat to a final thickness of 1.2 mm with uniform surface finish on planes (020) and (0 $\bar{2}$ 0). Since the optical absorption of PDPHB was low, a very thin layer of carbon black from a benzene flame (whose contribution to the signal was negligible) was carefully coated onto the (020) plane of the prepared sample i.e., the plane to be illuminated, to enhance its optical absorption. The output signal was measured using a lock-in amplifier (Stanford Research Systems, Model: No. SR830) with 10 MΩ input impedance and 50 pF input capacitance. The frequency of modulation of the laser source was kept in the range of 60–80 Hz to ensure that the detector, the sample, and the backing medium were all thermally thick during measurements. The thermal thickness of PDPHB was estimated by plotting the PPE amplitude and phase with different frequencies at room temperature and the results are shown in Fig. 5. Measurement of the PPE signal phase and amplitude enabled us to determine the thermal diffusivity ( $\alpha$ ) and thermal effusivity ( $e$ ) or heat penetration coefficient of the sample. From these measured values of  $\alpha$  and  $e$ , thermal conductivity ( $K$ ) and heat capacity ( $C_p$ ) were evaluated by the following relations,

$$K_s(T) = e_s(T) \cdot \sqrt{\alpha_s(T)}$$

$$C_{P_s} = \frac{e_s(T)}{\rho_s(T) \cdot \sqrt{\alpha_s(T)}}$$

where  $C_{P_s}$  is the heat capacity (at constant pressure) and  $\rho_s$  is the density of the sample, and are presented in Table 1. After repeated tests on several samples of known thermal properties, the uncertainty in the measured values of  $K$  and  $C_p$  was estimated to be less than 2%. The sample temperature was kept constant during the measurements, allowing sufficient time for the sample to reach thermal equilibrium. The results obtained through PPE analysis are

**Table 1** Comparison of thermal parameters of PDPHB with few known NLO crystals

Sample	Thermal effusivity/ $e \text{ W s}^{-1/2} \text{ m}^{-2} \text{ K}^{-1}$	Thermal diffusivity/ $\alpha \times 10^{-6} \text{ m}^{-2} \text{ s}^{-1}$	Thermal conductivity/ $\text{K W}^{-1} \text{ mK}^{-1}$	Specific heat capacity/ $C_p \text{ J}^{-1} \text{ g}^{-1} \text{ K}^{-1}$
Literature/20-29				
KDP	–	–	1.21/302 K	0.857/298 K
KTP	–	–	2	0.688/300 K
ADP	–	–	1.26/315 K	1.236/298 K
BBO	–	–	1.2	0.490/298 K
LAP	–	–	0.59	0.552
EMPO	660	2.773	1.099	0.443
BEDO	669	3.131	1.185	0.322
EDMP·3H <sub>2</sub> O	661	1.744	0.873	0.716
MDMP·3H <sub>2</sub> O	663	1.804	0.891	0.706
DMAPDP	663	2.951	1.14	0.332
2A5NPT	3216	2.561	5.143	1.283
NPNa·2H <sub>2</sub> O	–	–	0.63	1.423
ULMA	–	0.32	0.541	1.104/303 K
Acetoacetanilide	–	–	–	1.08/320 K
LN	–	–	–	0.648/300 K
DAPNP	–	–	–	1.278/298 K
LHPP	–	–	–	1.117/298 K
PDPHB/Present study	3162 ± 37	0.322 ± 0.0391	1.790 ± 0.103	4.6472 ± 0.0845/300 K

*KDP* potassium dihydrogen orthophosphate, *KTP* potassium titanyl phosphate, *ADP* ammonium dihydrogen phosphate, *BBO* beta-barium borate, *LN* lithium niobate, *EMPO* 3-[(1*E*)-*N*-ethylethanimidoyl]-4-hydroxy-6-methyl-2H-pyran-2-one, *BEDO* bis-2,7-diethylaminohepta-2,5-dien-4-one, *EDMP·3H<sub>2</sub>O* 1-ethyl-2,6-dimethyl-4(1H)-pyridinone trihydrate, *MDMP·3H<sub>2</sub>O* 1-methyl-2,6-dimethyl-4(1H)-pyridinone trihydrate, *DMAPDP* 4-dimethylaminopyridinium dihydrogen phosphate, *2A5NPT* 2-amino-5-nitropyridinium-toluenesulfonate, *LAP* L-arginine phosphate monohydrate, *LHPP* L-histidinium-4-nitrophenolate 4-nitrophenol, *DAPNP* 2,6-diaminopyridinium 4-nitrophenolate 4-nitrophenol, *NPNa·2H<sub>2</sub>O* sodium *p*-nitrophenolate dehydrate, *ULMA* urea L-malic acid

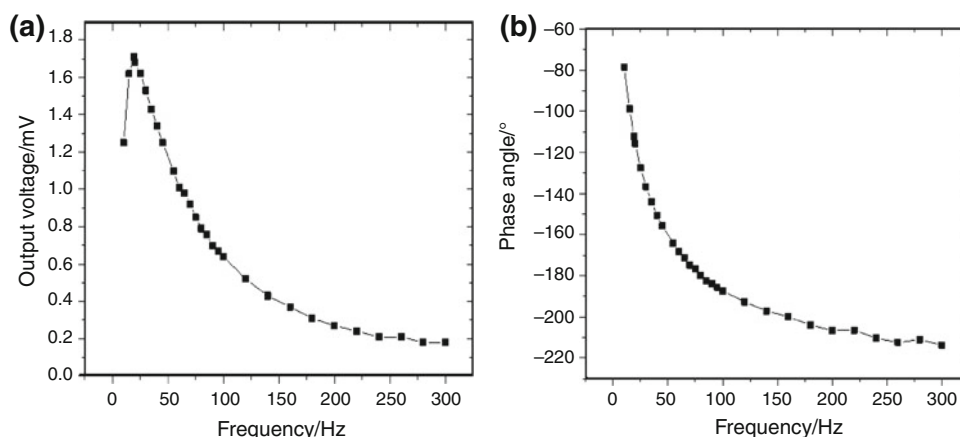
compared with few known NLO crystals [27] and are listed in Table 1. The thermal diffusivity of PDPHB was found to be about  $0.322 \times 10^{-6} \text{ m}^2 \text{ s}^{-1}$  which is lower than those of all the listed NLO crystals in Table 1 except ULMA ( $0.320 \times 10^{-6} \text{ m}^2 \text{ s}^{-1}$ ) which is comparable to it. The thermal diffusivity is of direct importance in heat flow studies, as it determines the rate of periodic heating or transient heat propagation through the medium, a situation often encountered in experiments with pulsed or chopped laser radiation. Physically, the inverse of thermal diffusivity is a measure of the time required to establish thermal equilibrium in a system for which a transient temperature change has occurred. The thermal effusivity, similar to thermal diffusivity, is a unique thermal property of a material and is one of the less explored quantities in physics. The major difference between the two is that diffusivity is a bulk property of the sample whereas the effusivity is relatively a surface property. The thermal effusivity essentially measures thermal impedance of the material, which in other words, is the ability of the sample to exchange heat with the environment. The thermal effusivity of PDPHB was found to be  $3162 \text{ W s}^{1/2} \text{ m}^{-2} \text{ K}^{-1}$  which was higher than those of all the organic dielectric

NLO crystals shown in Table 1, except 2A5NPT which is having comparably higher value ( $3216 \text{ W s}^{1/2} \text{ m}^{-2} \text{ K}^{-1}$ ) than PDPHB. The thermal conductivity of PDPHB was measured to be  $1.790 \text{ W mK}^{-1}$  along (020) direction. It is observed that this value is larger than that of the organic dielectric NLO crystals listed in Table 1, except 2A5NPT which is having comparably higher value ( $5.143 \text{ W mK}^{-1}$ ) than PDPHB.

### Dielectric Studies

Knowledge regarding the electric field distribution inside the material and the computation of electro optic and polarization optic coefficients is essential to realize the suitability of the NLO materials for the device applications [28]. Dielectric constant or relative permittivity ( $\epsilon_r$ ) of a dielectric material is a measure of the extent to which it concentrates electrostatic lines of force and the dissipation factor ( $D$ ) is a quantitative measure of the electromagnetic field that is absorbed or lost while traveling through a dielectric medium. A desirable property of a dielectric material is its ability to endure an electrostatic field while dissipating minimal energy in the form of heat. The lower

**Fig. 5** Variation of PPE **a** output voltage and **b** phase angle with frequency



the dielectric loss (i.e., the proportion of energy lost as heat), the more effective is a dielectric material and the crystals with high dielectric constant lead to greater power dissipation. In this view, the organic molecular crystals with relatively lower dielectric constant and dissipation factor as compared to their inorganic counter parts are useful in designing a circuit to operate at various frequencies. Besides the exploitation of crystals with positive dielectric constant as waveguides, optical filters and polarizers, devices made of these materials exhibit low dissipation up to optical frequencies, in contrast to metals, which are good only in the microwave regime ( $\lambda \approx 0.001$ – $0.3$  m), but suffer more losses at high frequencies (like visible light,  $\lambda \approx 3.8 \times 10^{-7}$ – $7.6 \times 10^{-7}$  m, for instance) [29]. To carry out the dielectric measurements, the two opposite flat faces  $\{(020)$  and  $(0\bar{2}0)\}$  of the freshly obtained PDPHB were carefully polished on a silk cloth with fine grade alumina powder dispersed in an ethanol medium so as to obtain a good surface finish. The polished samples of thickness 1 mm and surface area  $42 \text{ mm}^2$  were electroded with conductive silver paste, to act as a parallel plate capacitor, with the crystal as a dielectric medium. The dielectric constant of PDPHB crystal was calculated by using the relation

$$\epsilon_r = Ct/\epsilon_0 A$$

where  $\epsilon_0$  is the permittivity of free space,  $t$  is the thickness of the sample,  $C$  is the capacitance, and  $A$  is the area of cross section [30]. The frequency dependences of the dielectric constant and dielectric loss at different temperatures are shown in Fig. 6. It is found that the dielectric constant of PDPHB is comparatively higher at low frequencies and it decreases with increasing frequency. At 100 Hz, for instance, the value of dielectric constant is found to be around 4.2 and it reaches the value as low as 1.4 at 1 MHz. In fact, the nature of the variation of dielectric constant with frequency indicates the type of polarization response (such as space charge, orientation, electronic and ionic polarization). It is observed

from the dielectric studies that the dielectric constants of PDPHB crystal were not exceeding 4.5 in all considered frequencies and temperatures. It is comparatively lower than the high efficient organic NLO and electro optic crystals DAST ( $\epsilon_r \approx 5.21$ ) [31, 32], OH1 ( $\epsilon_r \approx 5.26$ ) [33], BNA ( $\epsilon_r \approx 3.902$ ) [34] and considerably lower than some inorganic electro optic crystals  $\text{LiNbO}_3$  ( $\epsilon_r \approx 85$ ) [35],  $\text{KNbO}_3$  ( $\epsilon_r \approx 154$ ) [36].

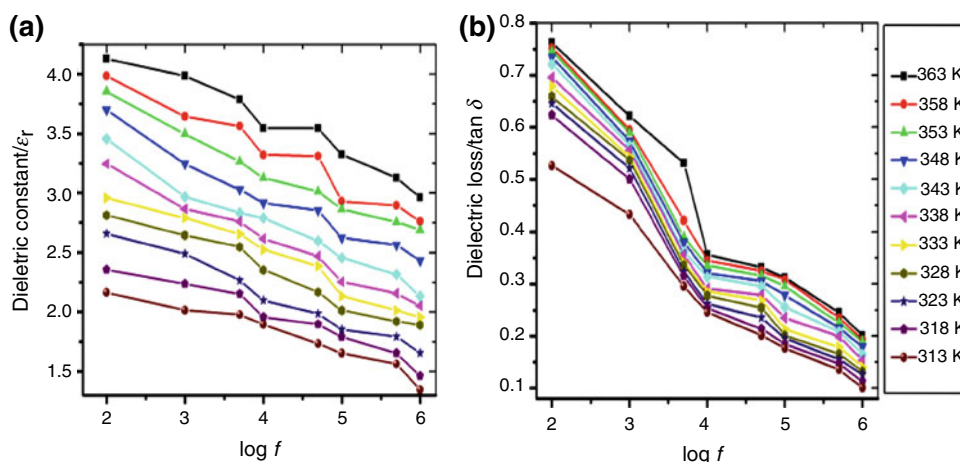
In general, substances with high dielectric constants tend to break down more easily when subjected to intense electric fields, than do materials with low dielectric constants. Organic crystals with low dielectric constant have wide spread applications in current research fields such as electro optic modulators (EOM), Non linear optical devices, THz wave generation, telecommunications, etc. [37–39]. The low dielectric constant of organic materials will also decrease the power requirement of EOM which is essential when building broadband EOM and field detectors. In PDPHB, both the dielectric constant and dielectric loss values were decreasing with increasing frequency and increasing with increasing temperature, with tolerable variations (Fig. 7). However, the variation of  $\epsilon_r$  with temperature is generally attributed to the crystal expansion, the electronic and ionic polarizations, and the presence of impurities and other crystal defects [37]. These kinds of materials, due to their feasible flat response with frequency variation, are always recognized to minimize the phase distortion caused by the vast change of dielectric constant follow-on the variation of frequency. Therefore, PDPHB crystal could be an interesting candidate for high speed applications in telecommunications provided that the optical wave guiding is achievable [40].

In addition to the dielectric measurements, the ac conductivity of PDPHB was also calculated using the formula,

$$\sigma_{ac} = \omega \epsilon_r \tan \delta \epsilon_0$$

(where  $\epsilon_0$  is the vacuum dielectric constant) at different temperatures. Figure 8a shows variation of ac conductivity

**Fig. 6** **a** Variation of dielectric constant and **b** loss versus frequency



with the temperature. It is evident from the graph that the conductivity increases with temperature. At lower temperature, the sample possesses minimum conduction, which may be due to minimum value of Gibbs free energy change [41]. As the electrical conduction in dielectrics is mainly a defect controlled process in low temperature region, the presence of impurities and vacancies predominantly determine this region. As the Gibbs energy is defined as the available energy to do a reaction, at low temperature, it is considered as minimum. It is also understood that in low temperature region, the energy needed to form the defect is much larger than the energy needed for its drift whereas at higher temperatures, the creation of electronic pathways increases the conductivity [42, 43]. The Arrhenius plot of  $\ln\sigma_{ac}T$  versus  $1000/T$  is shown in Fig. 8b. The activation energy for ionic migration was estimated from the graph. The line of best fit for the plot of  $\ln\sigma_{ac}T$  versus  $1000/T$  obeys Arrhenius relationship,

$$\sigma_{ac} = \sigma_0 \exp\left(-\frac{E_{ac}}{kT}\right)$$

where  $\sigma_0$  is the pre-exponent factor,  $E_{ac}$  is the activation energy for the ionic conduction process, and  $k$  is the

Boltzmann constant. Hence it could be stated that the sample exhibited Arrhenius type of conductivity behavior in the temperature range of investigation. The activation energy of PDPHB, for the thermally activated charge transport or conduction process was calculated from Fig. 8b and was found to be 0.21 eV [43].

#### Mechanical studies

The hardness of a material may be defined as the resistance it offers to the motion of dislocations, deformation, or to damage under an applied stress. Among various types of available hardness tests, Vickers hardness technique is an appropriate one for measuring the hardness of a thin layer (such as an electroplated layer) or for testing brittle materials where the tendency for fracture is proportional to the volume of stressed material. In order to measure the hardness of PDPHB, visibly crack or inclusion free transparent single crystal with dimensions of  $12 \times 8.5 \times 6.5$  mm ( $l \times b \times h$ ) was selected. To check the anisotropic nature, if any, of PDPHB, the hardness test was performed on the (020), (002), and (200) planes using Vickers hardness

**Fig. 7** **a** Variation of dielectric constant and **b** loss versus temperature

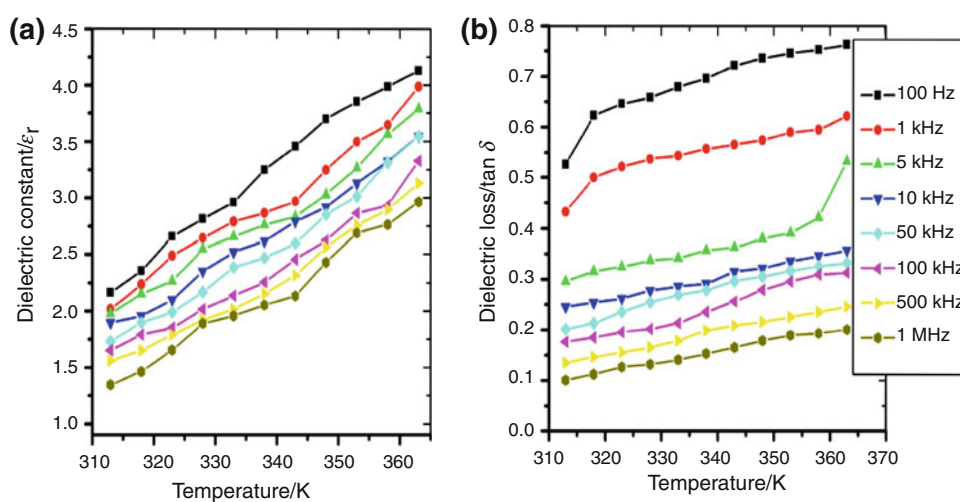


**Fig. 8** **a** Current conductivity behavior and **b** activation energy calculation of PDPHB single crystal

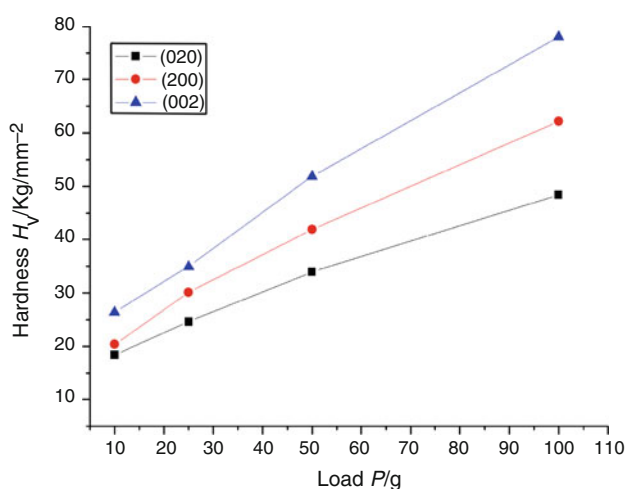
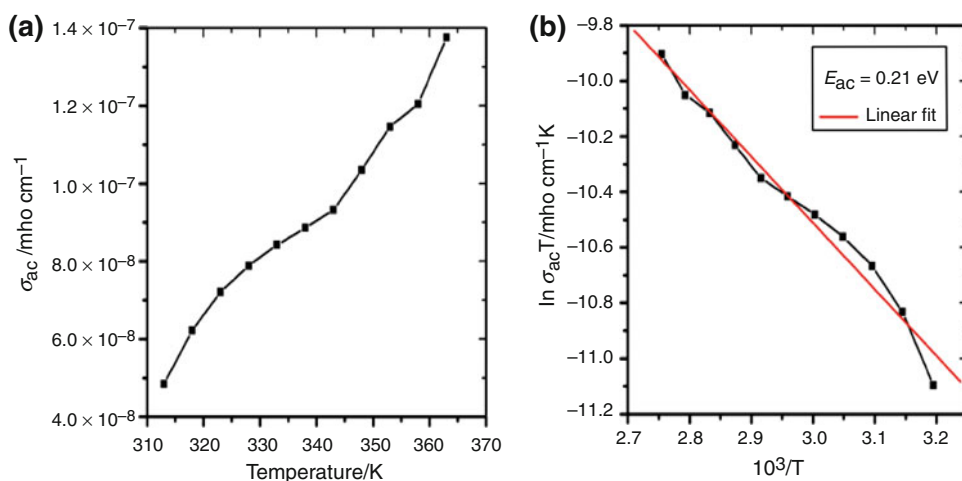


**Fig. 9** Hardness profile of PDPHB single crystal against Vickers indentation

indenter for the applied loads ranging from 10 to 100 g. The dwell time for each load was fixed as 10 s. Four indentations were made for each load, and the average diagonal length of the indented impressions was calculated. The surface area and volume of the sample were calculated as 4.705 cm<sup>2</sup> and 0.663 cm<sup>3</sup>, respectively. The Vicker’s hardness number ( $H_v$ ) of PDPHB was calculated using the expression

$$H_v = 1.854 \frac{P}{d^2}$$

where  $H_v$  is the Vicker’s hardness number in kg mm<sup>2</sup>,  $P$  is the applied load in kg, and  $d$  is the average diagonal length of the indentation in mm. The calculated values of  $H_v$  for various loads corresponding to each orientation are plotted as given in Fig. 9. Maximum indenter load applied for PDPHB crystal was 100 g, and above this load, micro-cracks were observed around the impression and hence readings were not taken for higher loads. From the figure, it could be seen that the microhardness number increases with increasing load in all orientations and this trend is termed as reverse indentation size effect (ISE) since the normal ISE usually involves a decrease in the apparent microhardness with increasing applied indentation load. This reverse ISE is normally obtained only in single crystals’ surfaces where plastic deformation is dominant [44–46]. The larger indentation size and hence the lower hardness values at low loads were due to the specimen’s relaxation through the release of the indentation stress away from the indentation site. This reverse ISE may have occurred due to the existence of a distorted zone near the crystal–medium interface; the effects of vibration and indenter bluntness at low loads; the applied energy loss as a result of specimen chipping around the indentation; the generation of median or radial

**Table 2** Anisotropic hardness behavior of PDPHB single crystal

Orientation	Hardness number $H_v$ for a load ( $9.8 \times 10^{-3}$ N) of				Work hardening coefficient ‘ $n$ ’
	10 g	25 g	50 g	100 g	
(200)	20.4	30.1	41.9	62.2	3.0135
(020)	18.4	24.6	33.9	48.4	2.1844
(002)	26.4	34.9	51.9	78	1.732



cracks during the indenter loading half-cycle; the relative predominance of nucleation and multiplication of dislocations; and the relative predominance of the activity of either two sets of slip planes of a particular slip system or two slip systems below and above a particular load [45, 46].

The relation connecting the applied load and diagonal length  $d$  of the indenter is given by the Meyer's law as,

$$P = ad^n$$

where  $n$  is the work hardening coefficient or Meyer's index that could be calculated from the slope of the straight line. The values of  $n$  obtained for PDPHB on various crystallographic planes are given in Table 2. Onitsch [47] has pointed out that  $n$  lies between 1.0 and 1.6 for hard materials whereas it is more than 1.6 for soft materials. Based on the above criterion, PDPHB could be considered as a soft material, in general [48]. The hardness value of PDPHB on (002) plane (50 g, 52 kg mm<sup>-2</sup>) is greater than the most important organic NLO crystal, DAST (50 g, 18 kg mm<sup>-2</sup>) [49], comparable to tri-nitrophenol methyl *p*-Hydroxybenzoate (50 g, 59 kg mm<sup>-2</sup>) [50] and lower than well-known inorganic NLO crystal KH<sub>2</sub>PO<sub>4</sub> (50 g, 173 kg mm<sup>-2</sup>) [51]. The relatively higher hardness values as compared to organic NLO crystals suggested that the average bond strength and the number of bonds per unit volume could be higher in PDPHB. The hardness values of PDPHB for various loads are given in Table 2. From the Table, it could be seen that the PDPHB exhibited anisotropic behavior in the measured planes and that hardness values on these planes were having the following order: (002) > (200) > (020). The direction dependent hardness values measured for PDPHB exhibit that it possesses anisotropic nature of bonding environment [52].

## Conclusions

Single crystals of PDPHB were grown using solution growth method. This compound was found to crystallize in monoclinic noncentrosymmetric space group Cc. The powder SHG efficiency was found to be about 19 times greater than that of KH<sub>2</sub>PO<sub>4</sub>. The TG/DTA curves verified the thermal stability of PDPHB up to its melting point (150 °C) whereas its purity and crystallinity were evidenced by the DSC curve through its sharp endothermic melting peak. The measured heat capacity by photopyroelectric technique, suggest that the PDPHB could possess high optical damage threshold value, which is an essential requirement in optical devices. The lower values of dielectric constant and loss favored the suitability of PDPHB for NLO applications. The Vickers microhardness test on (200), (020), and (002) planes revealed the anisotropic nature of PDPHB while reverse indentation size effects were observed against indentation loads.

**Acknowledgments** The authors hereby acknowledge the Department of Science and Technology (DST), New Delhi, India for the financial support through the DST-SERB project (SR/S2/CMP-0028/2011, Dated 01-12-2011).

## References

- Chen T, Sun Z, Song C, Ge Y, Luo J, Lin W, Hong M. Bulk crystal growth and optical and thermal properties of the nonlinear optical crystal 1-histidinium-4-nitrophenolate 4-nitrophenol (LHPP). *Cryst Growth Des.* 2012;12:2673–8.
- Alosious Gonsago C, Merina Albert H, Umamaheswari R, Joseph Arul Pragasam A. Spectral, optical, and thermal studies of pure and Zn(II)-doped L-histidine hydrochloride monohydrate (LHHC) crystals. *J Therm Anal Calorim.* 2012;110:839–45.
- Janarthanan S, Sugaraj Samuel R, Rajan YC, Umarani PR, Pandi S. Spectral and thermal characterization of grown organic single crystal Semicarbazone of *p*-hydroxy benzaldehyde (SPHB). *J Therm Anal Calorim.* 2012;109:69–72.
- Brahadeeswaran S, Onduka S, Takagi M, Takahashi Y, Adachi H, Kamimura T, Yoshimura M, Mori Y, Yoshida K, Sasaki T. Twin-free and high-quality DAST crystals—effected through solutions of lower supersaturation coupled with isothermal solvent evaporation. *Cryst Growth Des.* 2006;6:2463–8.
- Shanmugam G, Thirupugalmani K, Kannan V, Brahadeeswaran S. Spectroscopic, quantum-chemical and X-ray diffraction studies of piperidinium *p*-hydroxybenzoate-combined experimental and theoretical studies on a novel NLO crystal. *Spectrochim Acta A.* 2013;106:175–84.
- Fukuyama K, Kashino S, Haisa M. *Acta Crystallogr B.* 1973; B29:2713–7.
- Shanmugam G, Ravi Kumar K, Sridhar B, Brahadeeswaran S. Synthesis, structure, Growth and characterization of a novel organic NLO single crystal: morpholin-4-ium *p*-aminobenzoate. *Mater Res Bull.* 2012;47:2315–23.
- Bottom R. Thermogravimetric analysis. In: Gabbot P, editor. Principles and applications of thermal analysis. UK: Blackwell; 2008. p. 88–118.
- Kwon OP, Kwon SJ, Jazbinsek M, Choubey A, Gramlich V, Gunter P. New organic nonlinear optical polyene crystals and their unusual phase transitions. *Adv Funct Mater.* 2007;17:1750–6.
- Hatakeyama T, Zhenhai Liu. Handbook of thermal analysis. Chichester: Wiley; 1998.
- Gabbot P. A practical introduction to differential scanning calorimetry. In: Gabbot P, editor. Principles and applications of thermal analysis. UK: Blackwell; 2008. p. 1–50.
- Glass AJ, Guenther AH. Laser induced damage of optical elements- a status report. *Appl Opt.* 1973;12:637–49.
- Petrov V, Zondy J, Bidault O, Isaenko L, Vedenyapin V, Yeliseyev A, Chen W, Tyazhev A, Lobanov S, Marchev G, Kolker D. Optical, thermal, electrical, damage, and phase-matching properties of lithium selenoindate. *J Opt Soc Am B.* 2010;27:1902–27.
- Saraswat S, Kushwaha SSS. Specific heat studies in a-Se and a-Se<sub>90</sub>M<sub>10</sub> (M = In, Sb, Te) alloys. *J Therm Anal Calorim.* 2009; 96:923–7.
- Sun ZH, Xu D, Wang XQ, Zhang GH, Yu G, Zhu LY, Fan HL. Growth and characterization of the nonlinear optical single crystal: L-lysiniun trifluoroacetate. *Mater Res Bull.* 2009;44:925–30.
- Verdonck E, Schaap K, Thomas LC. A discussion of the principles and applications of modulated temperature DSC (MTDSC). *Int J Pharm.* 1999;192:3–20.
- Kong H, Wang J, Zhang H, Yin X, Zhang S, Liu Y, Cheng X, Gao L, Hu X, Jiang M. Growth, properties and application as an electrooptic Q-switch of langasite crystal. *J Cryst Growth.* 2003; 254:360–7.

18. Hou WB, Yang ZH, Liu MG, Yuan DR, Xu D, Zhang N, Yu WT, Bing YH, Sun SY, Tao XT, Jiang MH. Thermal properties of a new organometallic nonlinear optical material triallylthiourea mercury bromide (ATMB). *Mater Lett.* 1994;18:207–10.
19. Takahashi Y, Onduka S, Brahadeeswaran S, Yoshimura M, Mori Y, Sasaki T. Development of DAST crystals with high damage tolerance. *Opt Mater.* 2007;30:116–8.
20. Chen T, Sun Z, Li L, Wang S, Wang Y, Luo J, Hong M. Growth and characterization of a nonlinear optical crystal. 2,6-diaminopyridinium 4-nitrophenolate 4-nitrophenol (DAPNP). *J Cryst Growth.* 2012;338:157–61.
21. Dhanaraj G, Srinivasan MR, Bhat HL, Jayanna HS, Subramanyam SV. Thermal and electrical properties of the novel organic nonlinear crystal L-arginine phosphate monohydrate. *J Appl Phys.* 1992;72:3464–7.
22. Vanishri S, Babureddy JN, Bhat HL, Ghosh S. Laser damage studies in nonlinear optical crystal sodium *p*-nitrophenolate dehydrate. *Appl Phys B Laser Opt.* 2007;88:457–61.
23. Vijayan N, Rani N, Bhagavannarayana G, Haranath D, Jayabharathi J, Wahab MA, Das S. Optical, elemental and structural analyses of acetoacetanilide single crystals for nonlinear optical applications. *Spectrochim Acta A.* 2012;93:75–80.
24. Zhang HJ, Jiang HD, Wang JY, Hu XB, Yu GW, Yu WT, Gao L, Liu JA, Zhang SJ, Jiang MH. Growth and characterization of LaCa<sub>4</sub>O(BO<sub>3</sub>)<sub>3</sub> crystal. *Appl Phys A.* 2004;78:889–93.
25. Philip J, Manjusha MV. Thermal transport across incommensurate phases in potassium selenate: photo-pyroelectric and calorimetric measurements. *J Phys: Condens Matter.* 2009;21:45901–7.
26. Menon CP, Philip J. Simultaneous determination of thermal conductivity and heat capacity near solid state phase transitions by a photopyroelectric technique. *Meas Sci Technol.* 2000;11:1744–9.
27. Anandha Babu G, Ramasamy P, Philip J. Studies on the growth and physical properties of nonlinear optical crystal: 2-amino-5-nitropyridinium-toluenesulfonate. *Mater Res Bull.* 2011;46:631–4.
28. Gunter P. Electro-optical properties of KNbO<sub>3</sub>. *Opt Commun.* 1974;11:285–90.
29. Khazhinsky MG. PhD Thesis. Western Michigan University. USA: 1997.
30. Anderson JC. *Dielectrics*. 1st ed. London: Wiley; 1964.
31. Pan F, Knopfle G, Bosshard Ch, Follonier S, Spreiter R, Wong MS, Gunter P. Electro-optic properties of the organic salt 4-*N,N*-dimethylamino-4'-*N'*-methyl-stilbazolium tosylate. *Appl Phys Lett.* 1996;69:13–5.
32. Spreiter R, Bosshard Ch, Pan F, Gunter P. High-frequency response and acoustic phonon contribution of the linear electro-optic effect in DAST. *Opt Lett.* 1997;22:564.
33. Hunziker C, Kwon SJ, Figi H, Jazbinsek M, Gunter P. Fabrication and phase modulation in organic single-crystalline configurationally locked, phenolic polyene OH1 waveguides. *Opt Express.* 2008;16:15903–14.
34. Kuroyanagi K, Fujiwara M, Hashimoto H, Takahashi H, Aoshima S, Tsuchiya Y. Determination of refractive indices and absorption coefficients of highly purified *n*-benzyl-2-methyl-4-nitroaniline crystal in terahertz frequency regime. *Jpn J Appl Phys.* 2006;45:L761–4.
35. Jazbinsek M, Zgonik M. Material tensor parameters of LiNbO<sub>3</sub> relevant for electro- and elasto-optics. *Appl Phys B.* 2002;74:407–14.
36. Zgonik M, Schlessler R, Biaggio I, Voit E, Tscherry J, Gunter P. Materials constants of KNbO<sub>3</sub> relevant for electro and acousto-optics. *J Appl Phys.* 1993;74:1287–97.
37. Hartley R. Base materials for high-speed, high frequency PCB boards. Proceedings of the PCB & a west conference, California, 2002.
38. Han PY, Tani M, Pan F, Zhang XC. Use of the organic crystal DAST for terahertz beam applications. *Opt Lett.* 2000;25:675–7.
39. Cross GH, Oldroyd AR, Worboys MR. The linear electro-optic response in crystals of 4-nitro-4'-methyl benzylidene aniline (NMBA). *Opt Commun.* 1990;74:425–9.
40. Mutter L, Guarino A, Jazbinsek M, Zgonik M, Gunter P, Dobeli M. Ion implanted optical waveguides in nonlinear optical organic crystal. *Opt Exp.* 2007;15:629–38.
41. Vetha Potheher I, Rajarajan K, Jeyasekaran R, Vimalan M, Yogam F, Sagayaraj P. Growth, optical, thermal, and conductivity behavior of nonlinear optical single crystals of CdHg (SCN)<sub>4</sub> (CH<sub>3</sub>OC<sub>2</sub>H<sub>5</sub>O). *J Therm Anal Calorim.* 2013;111:1491–7.
42. Perumal S, Mahadevan CK. Growth and characterization of multiphased mixed crystals of KCl, KBr and KI-Part 2: electrical measurements. *Phys B.* 2005;367:172–81.
43. Vimalan M, Rajeshkumar T, Tamilselvan S, Sagayaraj P, Mahadevan CK. Growth and properties of novel organic nonlinear optical crystal: l-alaninium tartrate (LAT). *Phys B.* 2010;405:3907–13.
44. Li H, Han YH, Bradt RC. Knoop microhardness of single crystal sulphur. *J Mater Sci.* 1994;29:5641–5.
45. Arora SK, Trivikarama Rao GS, Batra NM. Vickers micromechanical indentation of BaMoO<sub>4</sub> crystals. *J Mater Sci.* 1984;19:297–302.
46. Sangwal K. On the reverse indentation size effect and microhardness measurement of solids. *Mater Chem Phys.* 2000;63:145–52.
47. Onitsch EM. Over the microhardness of the metals. *Mikroskopie.* 1947;2:131–51.
48. Malliga P, Alosious Gonsago C, Sagayaraj P, Joseph Arul Pragasam A. Crystal growth, spectral, optical, and thermal characterization of glycyl-L-alanine hydrochloride (GLAH) single crystal. *J Therm Anal Calorim.* 2012;110:873–8.
49. Haja Hameed AS, Rohani S, Yu WC, Tai CY, Lan CW. Surface defects and mechanical hardness of rapidly grown DAST crystals. *J Cryst Growth.* 2006;297:146–51.
50. Uthrakumar R, Vesta C, Robert R, Mangalam G, Jerome Das S. Optical and mechanical studies on unidirectional grown trinitrophenol methyl *p*-hydroxybenzoate bulk single crystal. *Phys B.* 2010;405:4274–8.
51. Fang T, Lambropoulos JC. Microhardness and indentation fracture of potassium dihydrogen phosphate (KDP). *J Am Chem Soc.* 2002;85:174–8.
52. Brahadeeswaran S, Bhat HL, Balaya P, Goyal PS. Dielectric, thermal, and mechanical properties of the semiorganic nonlinear optical crystal sodium *p*-nitrophenolate dihydrate. *J Appl Phys.* 2000;88:5935–40.